Supporting Information

Behabadi and Mel 10.1073/pnas.1217645111

SI Materials and Methods

Biophysical Model. The compartmental model was the same as that used in an earlier publication (1, ModelDB accession number 151404). All simulations were performed in NEURON (2) on a reconstructed layer 5 neocortical pyramidal cell morphology (3, 4).

Excitation was delivered at varying distances from the soma through combined NMDA receptor (R)/AMPAR-type synapses. The AMPA and NMDA component in each synapse had a fixed peak conductance (Table S1). Values were fit based on measured physiological summation nonlinearities (5). Both AMPA and NMDA conductances were modeled as difference-of-exponential functions with kinetics appropriate for 35 °C (Table S1). The NMDA channel model included an instantaneous voltage-dependent Mg-block of the form $B(V) = 1/(1 + e^{-(V+12)/10})$. Hodgkin–Huxley style sodium and potassium conductances were included in the axon, soma, and dendrites, with the sodium conductance decreasing linearly to 0 at a distance of 200 μm from the soma (6).

Synapse clusters were centered at specified locations with 0.5-μm spacing (7). Terminal dendrites were corrected for the membrane area contribution of unmodeled spines by increasing membrane capacitance and conductance by a factor of 2.0 (7). In simulations with NMDAR blocker 2-amino-5-phosphonovaleric acid (APV), the NMDA channel peak conductance was set to 0.

The axon, soma, and all dendritic subtrees containing activated synapses were divided into electrical compartments or "segments" of length no greater than one-tenth of the section's length constant at 100 Hz (8) or 10 μm, whichever was smaller. In other dendrites, three segments were used per section without loss of simulation accuracy.

Synaptic excitation was in the form of unsynchronized 50-Hz Poisson trains. Spike rates were averaged over the 500-ms stimulus period.

The Two-Layer Model and Linear Regression Parameter Estimation. The two-layer model was: $f(\boldsymbol{x}) = S\left(\sum_i D_i(x_i) + I_0\right)$, where f is the firing rate, $\boldsymbol{x}$ is the ensemble input configuration, S is the somatic f-I curve, D_i is dendrite i's current i/o function, and x_i is the input configuration in dendrite i. The dendritic currents from each branch were estimated using the following equation: $I_{total} = I_A + I_B + I_0$, where I_A and I_B are the dendritic currents from branch A and B, respectively, and I_0 is an offset current. I_{total} was found using a reverse lookup of the measured f-I function (S) for all nonzero firing rate results. For example, in Fig. 2 there were $40 \times 20 = 800$ input configurations, thus there were 800 equations with $40 + 20 + 1 = 61$ unknown parameters ($D_i(x_i)$, 40 input levels for I_B, 20 input levels for I_A, and the current offset I_0), which were solved by least squares linear regression.

1. Behabadi BF, Polsky A, Jadi M, Schiller J, Mel BW (2012) Location-dependent excitatory synaptic interactions in pyramidal neuron dendrites. *PLOS Comput Biol* 8(7):e1002599.
2. Carnevale NT, Hines ML (2006) *The NEURON Book* (Cambridge University Press, Cambridge, UK).
3. Behabadi BF, Mel BW (2007) J4 at sweet 16: A new wrinkle? *Neural Comput* 19(11): 2865–2870.
4. Douglas RJ, Martin KA, Whitteridge D (1991) An intracellular analysis of the visual responses of neurones in cat visual cortex. *J Physiol* 440:659–696.
5. Polsky A, Mel BW, Schiller J (2004) Computational subunits in thin dendrites of pyramidal cells. *Nat Neurosci* 7(6):621–627.
6. Nevian T, Larkum ME, Polsky A, Schiller J (2007) Properties of basal dendrites of layer 5 pyramidal neurons: A direct patch-clamp recording study. *Nat Neurosci* 10(2):206–214.
7. Larkman AU (1991) Dendritic morphology of pyramidal neurones of the visual cortex of the rat: III. Spine distributions. *J Comp Neurol* 306(2):332–343.
8. Hines ML, Carnevale NT (2001) NEURON: A tool for neuroscientists. *Neuroscientist* 7(2): 123–135.

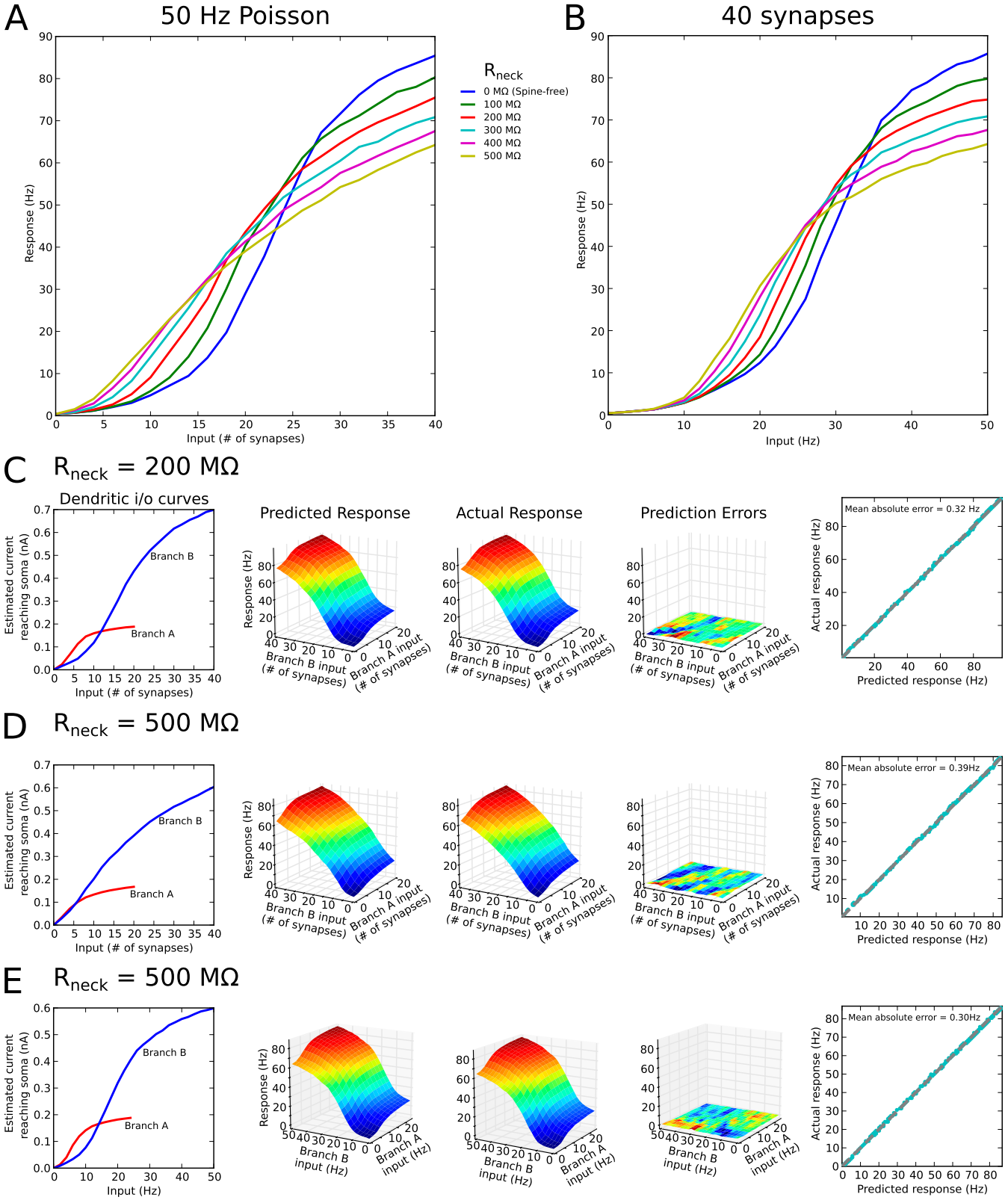

Fig. S1. Related to Fig. 2. Two-layer behavior does not depend on spine neck resistance. (*A*) Progression of dendritic input–output curves for increasing spine neck resistance. Synaptic inputs were centered 90 μm from the soma, at the same location as the proximal input in Fig. 2. Increasing spine neck resistance led to a lowered threshold (i.e., left shifting) of the i/o curves and tended to linearize their sigmoidal shape. The 0 MΩ blue curve in *A* is the same as in Fig. 2*E*. (*B*) Similar to *A*, but replacing synapse count (at 50 Hz) with input frequency (for 40 synapses) as the measure of input intensity. Increasing spine neck resistance again lowered thresholds, but preserved the input–output curves' sigmoidal shape. (*C*–*E*). The simulations of Fig. 2 were repeated using spines with 200 MΩ and 500 MΩ neck resistances with fixed-frequency (*C* and *D*) and fixed-synapse (*E*) input. Prediction errors were very small in all cases.

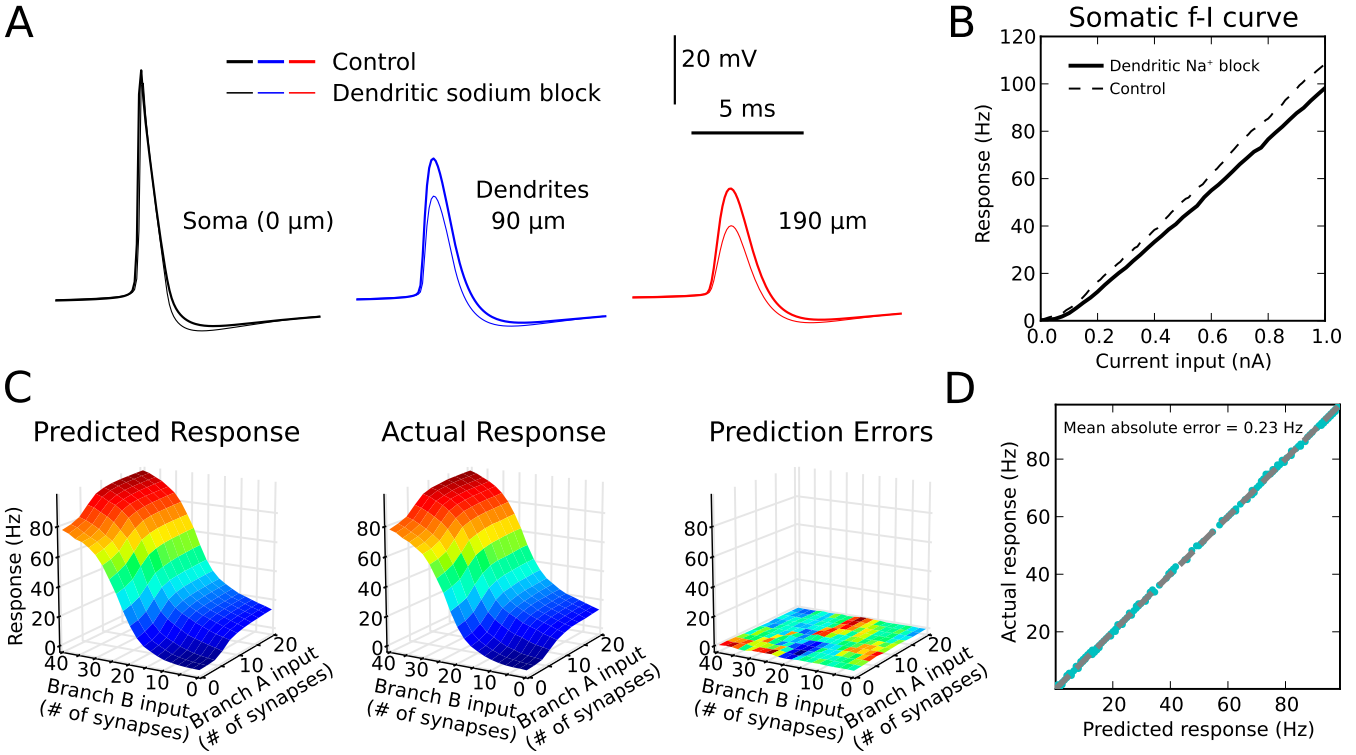

Fig. S2. Related to Fig. 2. Quantifying subunit independence with dendritic sodium block. Same configuration and format as in Fig. 2, with some figure panels omitted. (*A*) Dendritic Na^+ channel block increases back-propagating action potential (bAP) attenuation along the length of the dendrite; compare thin (dendritic Na^+ block) and thick (control) curves. (*B*) Dendritic Na^+ channel block slightly reduced the neuron's excitability as shown by the decreased f-I slope. (*C*) Predicted (*Left*) and actual responses (*Center*) in the dendritic sodium block experiment were nearly identical. Prediction errors (*Right*) ranged from −0.7 Hz to + 0.9 Hz, with a mean of 0.23 Hz. These are slightly improved compared with the control condition in Fig. 2*D* (−1.2 Hz to +1.6 Hz; mean absolute error, MAE = 0.32 Hz). (*D*) Scatterplot of actual vs. predicted firing rates.

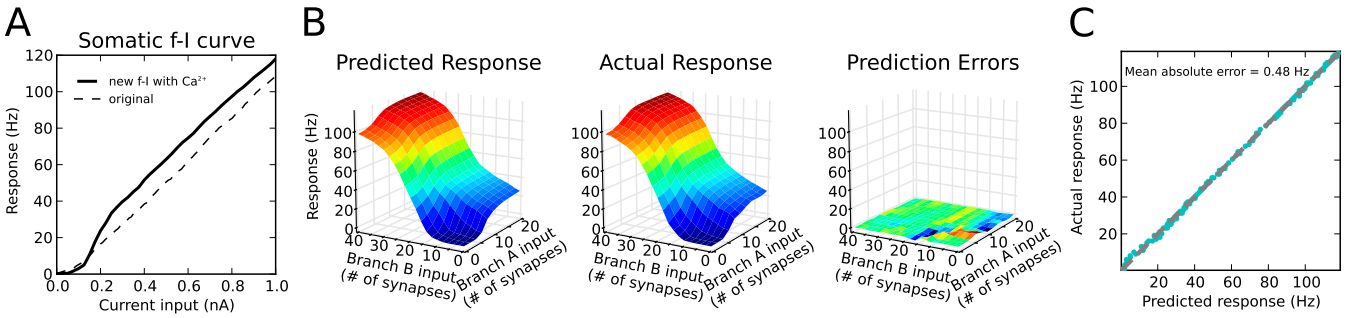

Fig. S3. Related to Fig. 2. Alteration of the somatic f-I curve by addition of a calcium spiking mechanism in the apical tree does not significantly disrupt subunit independence. Same configuration and format as in Fig. 2, with some figure panels omitted. (*A*) Voltage-dependent calcium channels were concentrated (0.0075 S/cm^2) around 600 µm from the soma (1). A dendritic current injection (0.625 nA) was used to prime the generation of calcium spikes, changing the gain of the somatic f-I curve (2). The somatic current injection representing background synaptic activation was lowered to a mean of 0.275 nA (from 0.75 nA), to compensate for the additional apical dendritic current injection. (*B*) Predicted (*Left*) and actual responses (*Center*) in the presence of the activated calcium spiking mechanism were nearly identical. Prediction errors (*Right*) ranged from −3 Hz to +3 Hz, with a mean of 0.48 Hz. (*C*) Scatterplot of actual vs. predicted firing rates.

1. Larkum ME, Nevian T, Sandler M, Polsky A, Schiller J (2009) Synaptic integration in tuft dendrites of layer 5 pyramidal neurons: A new unifying principle. *Science* 325(5941):756–760.
2. Larkum ME, Senn W, Lüscher H-R (2004) Top-down dendritic input increases the gain of layer 5 pyramidal neurons. *Cereb Cortex* 14(10):1059–1070.

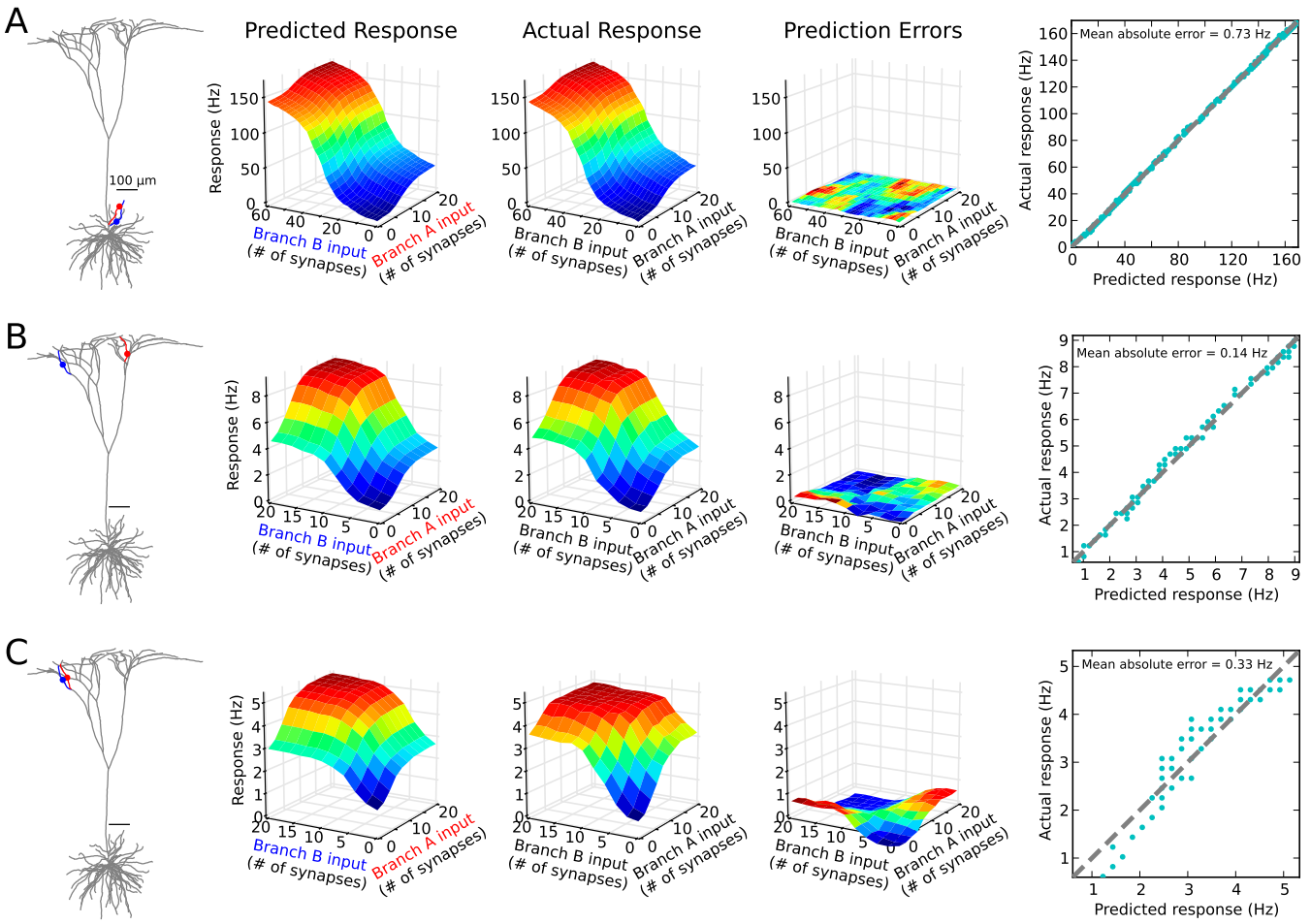

Fig. S4. Related to Fig. 2. Two-layer integration in nonbasal dendrites. Similar format to Fig. 2 with some figure panels removed. (*A*) Summation between a pair of oblique dendrites attached to the apical trunk with stimulation sites 90 and 190 μm from the cell body. Mean absolute error (MAE) of predictions was less than 1 spike per second (0.73 Hz). (*B*) Summation between a cousin pair of apical tuft dendrites. Stimulation was 960 μm from the cell body at both sites. In this case each input alone could only evoke ~4 Hz at the cell body. MAE was 0.14 Hz. (*C*) Summation between a sister pair of apical tuft dendrites. Stimulation was 960 μm from the cell body at both sites. Each input alone evoked ~3 Hz at the cell body. MAE was 0.33 Hz. Subunit isolation and hence prediction errors were worse than in the cousin branch case in *B*, consistent with findings from the basal dendrites (Fig. 2*F*).

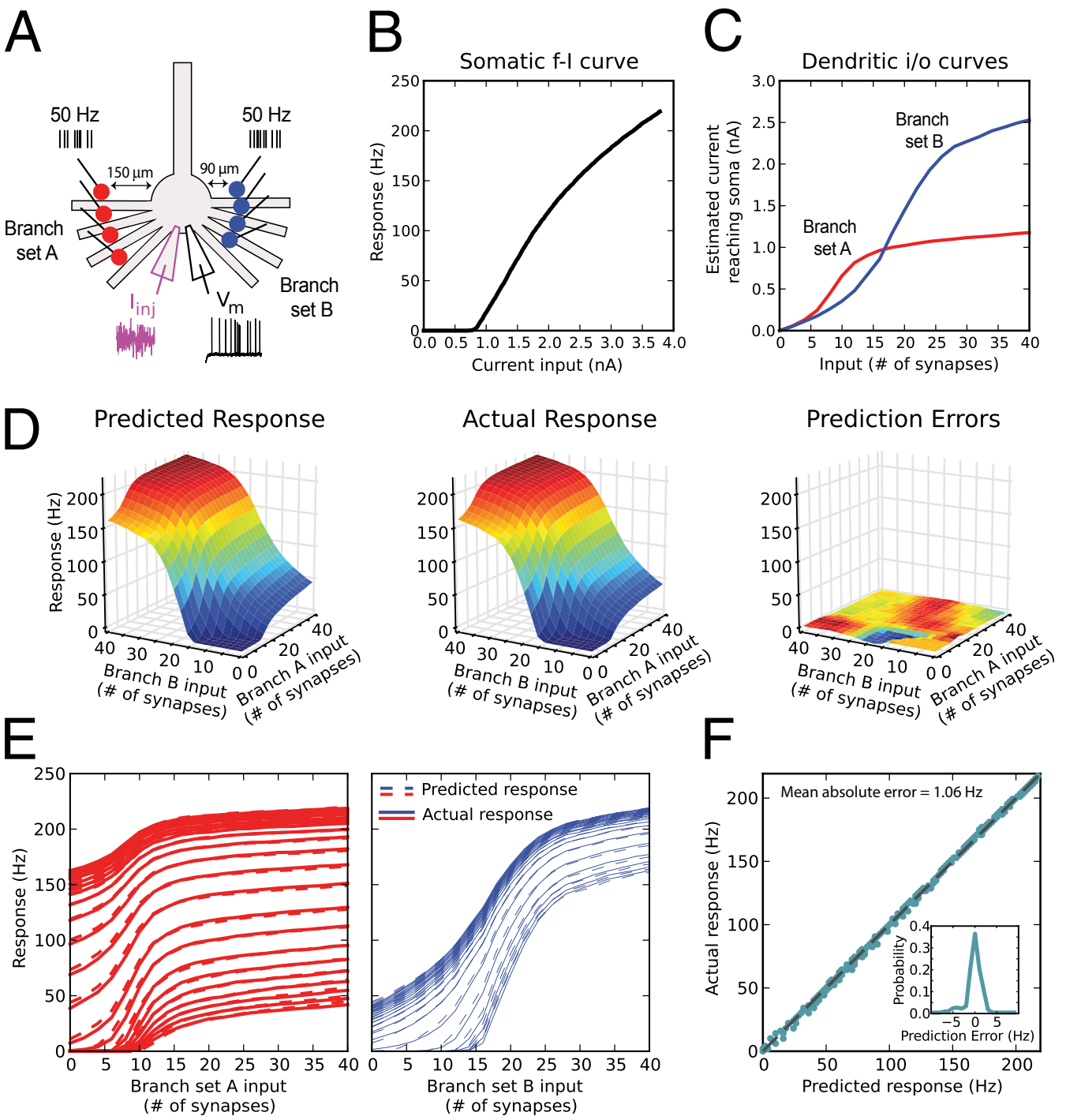

Fig. S5. Related to Fig. 2. Quantifying subunit independence with intense dendritic stimulation and a nonlinear somatic f-I curve. (*A* and *B*) Simulation experiments were as in Fig. 2, except (*i*) synaptic excitation was delivered to two sets of four dendrites (*A*), and (*ii*) the somatic current injection representing background synaptic activation was shifted down to a zero mean, leading to a deep resting potential and nonlinear somatic f-I curve (*B*). Branch set A inputs were moved closer to the soma, 150 µm away, to effectively drive the cell alone. (*C*) Current estimates for branch set A and branch set B from the regression fit to actual response. (*D*) Predicted (*Left*) and actual responses (*Center*) were again nearly identical. Prediction errors (*Right*) ranged from −7 Hz to +3 Hz. (*E*) Superimposed slices of 3D graphs in *D* show level-by-level comparisons of predicted and actual firing rates. (*F*) Scatterplot of actual vs. predicted firing rates as in Fig. 2 (MAE = 1.06 Hz). (*Inset*) Probability density of prediction errors over all 1,600 combinations of stimulus intensities. (*Left*) Skew of prediction error distribution corresponds to the blue region in *D*, *Right*, with maximum breakdown of subunit independence near somatic firing threshold.

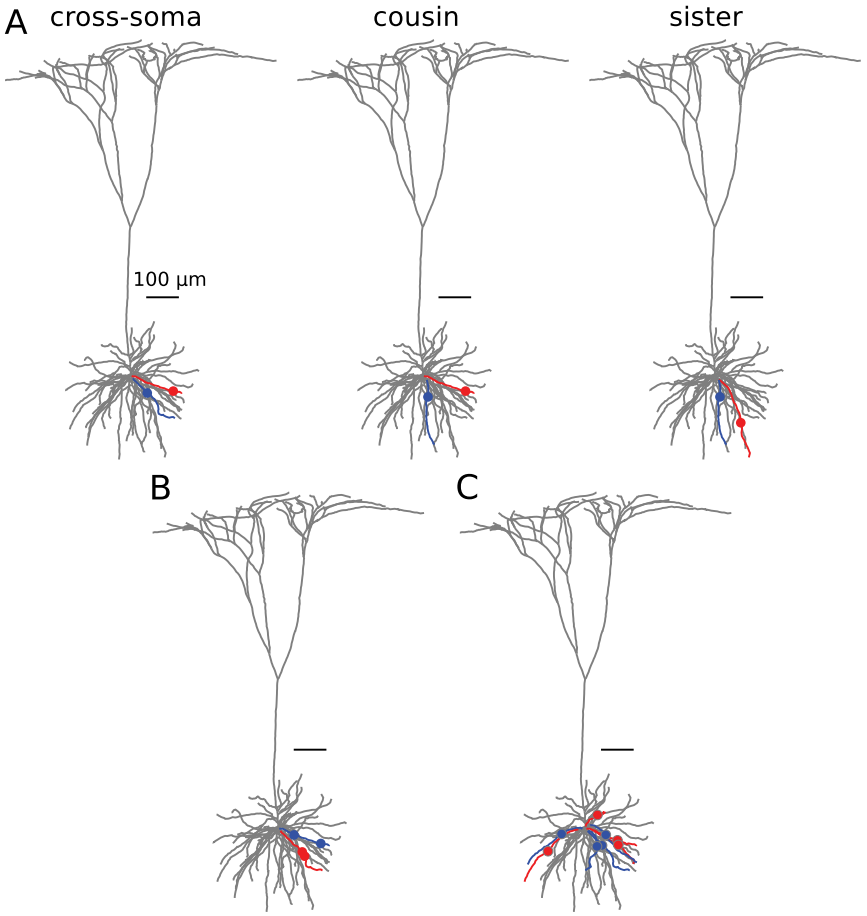

Fig. S6. Related to Figs. 2 and 3 and Figs. S1–S3 and S5. Synaptic input configurations shown on the reconstructed pyramidal neuron morphology. All dendrites are colored gray, except the highlighted branches receiving stimulation at the sites indicated by the colored balls (color scheme matches the related figures). It is important to note that the morphology has dendrites that extend into all three dimensions, so that it can be difficult to infer nearness of synapses in this 2D view of the cell. (*A*) Two-input, two-branch configurations for cross-soma (Fig. 2 and Figs. S1–S3), and cousin and sister dendrite pair simulation experiments (Fig. 2*F*). (*B*) Four-input, two-branch simulation experiment in Fig. 3. (*C*) Eight-input, eight-branch (two-branch set) simulation experiment in Fig. S5.

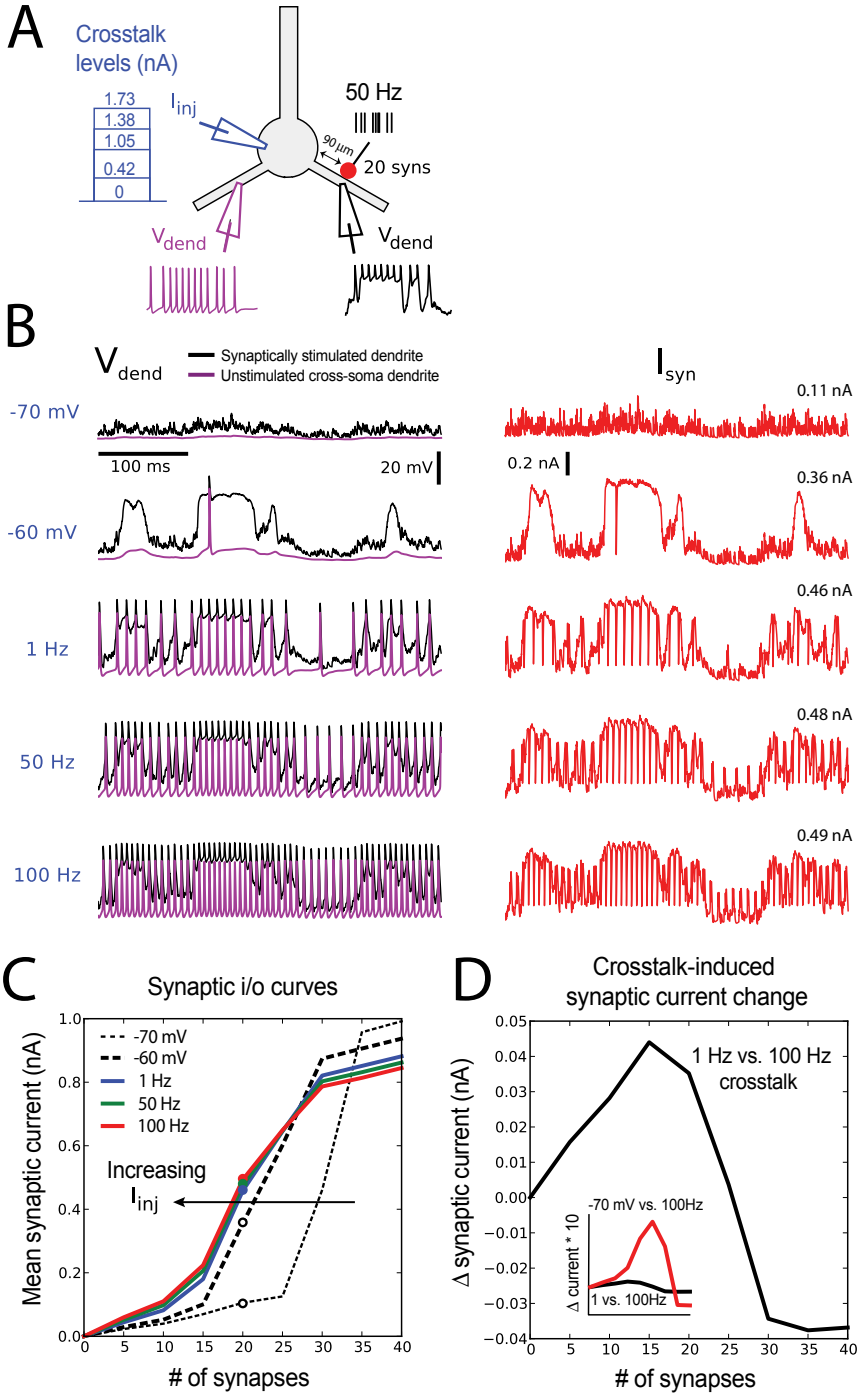

Fig. S7. Related to Fig. 4. Analysis of synaptic conductances, currents, and voltages for sub- and suprathreshold current injections. (*A*) Schematic of simulation runs with different steady current injections at the soma, 0, 0.42, 1.05, 1.38, and 1.73 nA, leading to subthreshold depolarizations with V_{dend} = −70 mV and V_{dend} = −60 mV as well as three suprathreshold cases with low (1 Hz), medium (50 Hz), and high (100 Hz) "cross-talk" bAP rates. The same synaptic input was used as in Fig. 4 *B* and *C*. (*B*) Dendritic voltage (*Left*) and synaptic current recordings (*Right*) for each of the five current injection levels. Purple voltage traces show the voltage response 90 μm from the soma in an unstimulated dendrite across the soma from the activated dendrite. Subthreshold depolarizations from the activated dendrite appear in attenuated form in the inactive dendrite, whereas the different suprathreshold responses are translated into different bAP rates with similar baseline depolarizations (around −55 mV). (*C*) Mean synaptic current for increasing somatic current injection levels. Note the tightly packed synaptic *i*/*o* curves for the three suprathreshold current injections and their similarity to the dendritic *i*/*o* curves in Fig. 2*C*. (*D*) Difference in synaptic *i*/*o* curves for low (1 Hz) and high (100 Hz) bAP rates. Maximal positive difference is 0.045 nA for 15 synapses (a "pure" down-state case) and the maximal negative difference is 0.37 nA for 35 synapses (a pure up-state configuration). (*Inset*) Comparison of cross-talk–induced current perturbations when cross-talk signals span range of 1–100 Hz (black original curve shown at different scale) vs. entire range from −70 mV to 100 Hz. Changes in synaptic currents are much larger in the latter case.

Table S1. Model parameters

	Property	Value	References
Passive properties	R_m	Dendrites: 10 kΩcm^2 Axon nodes: 50 Ωcm^2 Other: 20 kΩcm^2	
	C_m	Dendrites: 2 μF/cm^2 Myelinated axon: 0.05 μF/cm^2 Other: 1 μF/cm^2	(1)
	R_a	100 Ωcm	
	E_{leak}	−70 mV	
Active properties	$\bar{g}_{Na}$	Dendrites: 0.006 S/cm^2 Nonmyelinated axon: 5 S/cm^2 Myelinated axon: 0.006 S/cm^2 Soma: 0.25 S/cm^2	(2)
	$\bar{g}_K$	Dendrites: 0.0003 S/cm^2 Nonmyelinated axon: 0.05 S/cm^2 Soma: 0.03 S/cm^2	(3)
	E_{Na}	+60 mV	
	E_K	−90 mV	
Synapses	AMPAR	g_{max} = 1.5 nS $\tau_{rise,fall}$ = 0.05, 0.5 ms	(2, 4, 5)
	NMDAR	g_{max} = 3.9 nS $\tau_{rise,fall}$ = 2.1, 18.8 ms	(6, 7–9)
	$E_{AMPA/NMDAR}$	0 mV	

1. Mainen ZF, Sejnowski TJ (1996) Influence of dendritic structure on firing pattern in model neocortical neurons. *Nature* 382(6589):363–366.
2. Nevian T, Larkum ME, Polsky A, Schiller J (2007) Properties of basal dendrites of layer 5 pyramidal neurons: A direct patch-clamp recording study. *Nat Neurosci* 10(2):206–214.
3. Poirazi P, Brannon T, Mel BW (2003) Pyramidal neuron as two-layer neural network. *Neuron* 37(6):989–999.
4. Forti L, Bossi M, Bergamaschi A, Villa A, Malgaroli A (1997) Loose-patch recordings of single quanta at individual hippocampal synapses. *Nature* 388(6645):874–878.
5. Smith MA, Ellis-Davies GC, Magee JC (2003) Mechanism of the distance-dependent scaling of Schaffer collateral synapses in rat CA1 pyramidal neurons. *J Physiol* 548(Pt 1):245–258.
6. Polsky A, Mel BW, Schiller J (2004) Computational subunits in thin dendrites of pyramidal cells. *Nat Neurosci* 7(6):621–627.
7. Destexhe A, Mainen ZF, Sejnowski TJ (1998) *Methods in Neuronal Modeling: From Ions to Networks*, eds Koch C, Segev I (MIT Press, Cambridge, MA), 2nd Ed, pp 1–25.
8. Mainen ZF, Malinow R, Svoboda K (1999) Synaptic calcium transients in single spines indicate that NMDA receptors are not saturated. *Nature* 399(6732):151–155.
9. Popescu G, Robert A, Howe JR, Auerbach A (2004) Reaction mechanism determines NMDA receptor response to repetitive stimulation. *Nature* 430(7001):790–793.